Interstitial zinc clusters in zinc oxide

M. A. Gluba, N. H. Nickel, and N. Karpensky
Helmholtz-Zentrum Berlin für Materialien und Energie Institut für Silizium Photovoltaik Kekuléstr. 5, 12489 Berlin, Germany
(Received 21 June 2013; published 10 December 2013)

Doped zinc oxide (ZnO) exhibits anomalous Raman modes in the range of 270 to 870 cm^{-1}. Commonly, the resonance at 275 cm^{-1} is attributed to the local vibration of Zn atoms in the vicinity of extrinsic dopants. We revisit this assignment by investigating the influence of isotopically purified zinc oxide thin films on the frequency of the vibrational mode around 275 cm^{-1}. For this purpose, undoped and nitrogen-doped ZnO thin-films with Zn isotope compositions of natural Zn, ^{64}Zn, ^{68}Zn, and a 1:1 mixture of ^{64}Zn and ^{68}Zn were grown by pulsed laser deposition. The isotopic shift and the line shape of the Raman resonance around 275 cm^{-1} are analyzed in terms of three different microscopic models, which involve the vibration of (i) interstitial zinc atoms bound to extrinsic defects, (ii) interstitial diatomic Zn molecules, and (iii) interstitial zinc clusters. The energy diagram of interstitial Zn-Zn bonds in a ZnO matrix is derived from density functional theory calculations. The interstitial Zn-Zn bond is stabilized by transferring electrons from the antibonding orbital into the ZnO conduction band. This mechanism facilitates the formation of interstitial Zn clusters and fosters the common *n*-type doping asymmetry of ZnO.

DOI: 10.1103/PhysRevB.88.245201 PACS number(s): 78.30.−j, 78.20.Bh

I. INTRODUCTION

Over the last decade zinc oxide (ZnO) has attracted considerable interest as a wide band-gap optoelectronic material for applications comprising transparent thin-film transistors for flat panel screens,[1,2] light-emitting devices,[3] and transparent conducting oxide layers in solar cells.[4] Despite of its implementation in numerous applications the major drawback of ZnO is the lack of stable *p*-type material. Commonly, ZnO exhibits *n*-type conductivity, which is attributed to the presence of hydrogen atoms that act as shallow donors[5–7] and native defects, such as interstitial Zn atoms.[8] To achieve *p*-type doping, group-V elements are incorporated during growth. Among those elements nitrogen is being favored because of its small size.

Previously, the influence of nitrogen on the ZnO lattice dynamics was investigated using Raman backscattering spectroscopy. In addition to the ZnO phonon modes, new vibrational modes in the range of 270–870 cm^{-1} were reported. The intensity of these modes was found to be proportional to the nitrogen concentration; hence, it was suggested that they were caused by nitrogen.[9] However, the same vibrational modes were also observed in ZnO doped with Ga, Fe, Sb, Li, and Al. Consequently, it was suggested that the additional Raman modes may be caused either by lattice distortions due to the dopants[10] or by a disorder-induced relaxation of the translational symmetry that allows the observation of the silent Raman *B* modes.[11]

For three of the additional modes, explicit microscopic models were derived that do *not* require a disorder-induced activation of the *B* modes. Performing Raman measurements with different excitation wavelengths showed that the vibrational mode at $\nu = 577$ cm^{-1} is due to resonantly enhanced longitudinal optical (LO) phonons. This extrinsic Fröhlich interaction allowed the observation of third- and fourth-order phonon scattering at $\nu = 1700$ and 2300 cm^{-1}.[12] The origin of the anomalous Raman modes located at $\nu \approx 274$ and 510 cm^{-1} was deduced from isotope experiments. For this purpose, ZnO films were grown with a natural zinc isotope distribution and with isotopically pure ^{68}Zn. Then the specimens were implanted with nitrogen. Since a nitrogen-related isotope effect was not observed,[13] the shift of the vibrational modes at $\nu \approx 274$ and 510 cm^{-1} to smaller wave numbers by $\Delta\nu = 5.4$ and 1.9 cm^{-1}, respectively, was attributed to an interstitial Zn atom bound to a substitutional nitrogen atom (Zn_i-N_O) and a Zn_i-O_i complex.[14]

In this paper, we revisit the anomalous vibrational mode located at $\nu \approx 274$ cm^{-1}. The microscopic model proposed by Friedrich *et al.* [14] can account for the vibrational mode in nitrogen-doped ZnO. However, the Raman line is also observed when other dopants, such as Al, Fe, and Sb, are present in ZnO.[10,15] Assuming that the vibrational mode originates from Zn_i dopant complexes, one would expect that the stretching frequency changes to some degree because of different bonding configurations for the various dopants. To elucidate this question, a detailed investigation of the influence of ^{64}Zn and ^{68}Zn isotopes on the phonon modes is presented. The isotopic shift and the linewidth of the vibrational mode unambiguously show that its origin is caused by small zinc clusters containing approximately nine atoms.

The paper is organized as follows. Sample growth and preparation and the characterization methods employed are described in Sec. II. This section also contains a short description of the parameters utilized for density functional theory (DFT) calculations. In Sec. III Raman backscattering data of natural and isotopically pure ZnO samples are presented. The implications of the data on possible microscopic models are discussed in detail in Sec. IV. Finally, the main conclusions of this work are summarized in Sec. V.

II. EXPERIMENTAL

Zinc oxide samples were grown by pulsed laser deposition (PLD) using a XeCl excimer laser with an excitation wavelength of 308 nm and a repetition rate of 10 Hz. The pulse length was about 100 ns. For the PLD growth-process, ceramic targets were produced by cold pressing ZnO with a pressure density of 108 kg/cm^2 and subsequently sintering the targets for 5 h at a temperature of 950 °C. Some targets were fabricated from isotopically enriched ^{64}ZnO and ^{68}ZnO powder with a

purity of 99.2 and 98%, respectively. The ZnO samples were grown on sapphire and silicon substrates using a power density of about 12.5 J/cm^2 at the target. The substrate to target distance was kept at 10 cm. The ZnO samples were deposited at a substrate temperature of 700 °C and had a thickness that varied between 0.5 and 1.0 μm. Some samples were grown using plasma-assisted PLD. For this purpose, monatomic oxygen from an optically isolated remote microwave plasma was added during the growth process. Nitrogen doping was achieved by adding a flow of N_2O gas and increasing the deposition pressure to 4×10^{-4} mbar. The samples were characterized employing Raman spectroscopy. The 488- and 514.5-nm lines of an Ar^+ ion laser were used to irradiate the ZnO specimens, and the scattered light was detected in the backscattering geometry. Measurements performed at low temperatures were carried out by mounting the samples in a continuous flow liquid-helium cryostat.

To elucidate the experimental results, DFT calculations were performed using the projector-augmented plane-wave approach. ZnO was modeled in a supercell geometry using up to 130 atoms. The *d* electrons of Zn were treated as valence electrons, and the calculations were carried out using the general gradient approximation (GGA) + U. Here, U reflects the onsite coulomb repulsion parameter.[16] The effective strength of the respective correlation and exchange was set to $U - J = 4.7$ eV.[17] A k-point mesh of $3 \times 3 \times 3$ and a plane-wave cutoff of 400 eV were used. The vibrational frequencies of various interstitial Zn complexes were calculated with the harmonic oscillator approach. For the calculation of energy levels the hybrid functional of Heyd, Scuseria, and Ernzerhof (HSE) were used.[18] This functional combines the GGA of Perdew, Burke, and Ernzerhof[19] with a Hartree-Fock exchange. To match the optical gap of ZnO, a mixing parameter of 0.36 was chosen. The DFT calculations were carried out using the Vienna *ab initio* Simulation Package.[20,21]

III. RESULTS

Figure 1 shows Raman spectra of ZnO layers deposited on single-crystal silicon (*c*-Si) substrates with and without an additional microwave-assisted oxygen plasma. The measurements were performed at room temperature. The spectra of both specimens exhibit the ZnO related E_2^{high} phonon at $\nu = 436.2$ cm^{-1} and the LO-TO phonon of the *c*-Si substrate at $\nu = 520$ cm^{-1}. The sample grown without an O_2 plasma shows additional vibrational modes at $\nu = 271.8$ and 577.0 cm^{-1}. Previously, the presence of the phonon mode at $\nu = 577.0$ cm^{-1} was ascribed to a resonant enhancement of the E_1 and A_1 LO phonons in ZnO. The origin of the Fröhlich scattering is attributed to the presence of localized states in the optical band gap of ZnO[12] and, thus, can be used as a measure of the quality of ZnO. The simultaneous observation of the local vibrational mode (LVM) at $\nu = 271.8$ cm^{-1} corroborates this conclusion, since this line was identified as the local vibration of interstitial zinc atoms[14] that act as shallow donors.[22] The large difference in the thermal expansion of Si and ZnO results in tensile-strained layers; hence, this vibrational mode is shifted to smaller wave numbers by about 3 cm^{-1}. However, when ZnO is deposited using plasma-assisted PLD, the additional vibrational modes are suppressed (see Fig. 1).

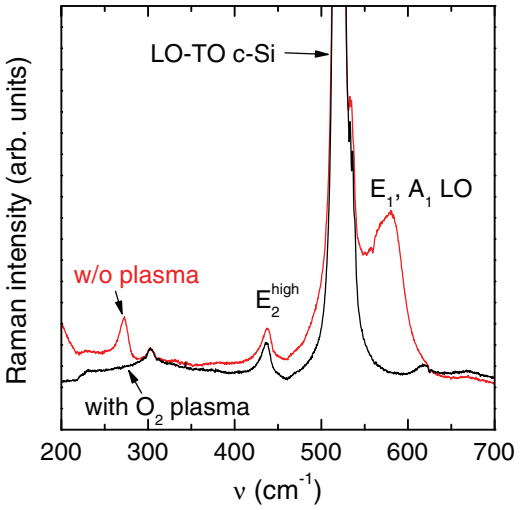

FIG. 1. (Color online) Raman backscattering spectra of undoped ZnO thin-films deposited on single-crystal silicon. Both specimens show the ZnO related E_2^{high} phonon mode and the LO-TO phonon mode of the silicon substrate. In addition, the specimen deposited without the presence of an O_2 plasma exhibits the E_1, A_1 LO phonon mode at $\nu = 577$ cm^{-1} and a vibrational mode at $\nu = 271.8$ cm^{-1}. The Raman measurements were performed at room temperature using an excitation wave length of 514.5 nm.

In the standard PLD process, ZnO is grown under Zn-rich conditions, leading to the incorporation of a large amount of interstitial Zn atoms. When adding monatomic O from the remote plasma, the ZnO growth conditions are shifted towards stoichiometric growth. As a result, the concentration of localized defects that give rise to the LO phonon mode and the amount of interstitial Zn are significantly reduced and can no longer be detected by Raman scattering experiments. This clearly shows that plasma-assisted PLD growth leads to structurally improved ZnO layers. Moreover, it demonstrates, that the Raman mode at $\nu = 271.8$ cm^{-1} can be observed without intentionally doping the ZnO films.

The LVM close to $\nu \approx 275$ cm^{-1} also has been observed in ZnO doped with various elements, such as Al, Ga, Sb, and N.[9,10,14] To elucidate the origin of the LVM, it is important to investigate the influence of the growth conditions on the Raman spectra. For this purpose, two *c* axis-oriented sapphire samples were placed into the PLD chamber. Then, one substrate was shielded from the plasma by a mechanical shutter, while a 200-nm-thick Al-doped ZnO layer was deposited. The Al concentration amounted to 2 at.%. Subsequently, the shutter was opened, and an undoped ZnO layer with a thickness of about 0.6 μm was deposited on both substrates. The Raman spectra of these samples are shown in Fig. 2. The specimen containing the Al-doped layer exhibits the LVM at $\nu \approx 274$ cm^{-1}, while the second sample that was directly grown on sapphire does *not* show this vibrational mode. Since ZnO crystallizes in a wurtzite structure with the *c* axis normal to the sapphire substrate, the surface can either be Zn- or O-terminated. Previously, it was shown that Al-doping causes a polarity change from a c(−) face to a c(+) face.[23] Hence, the data shown in Fig. 2 clearly shows that the presence of the LVM at $\nu \approx 274$ cm^{-1} is directly related to the surface polarity of ZnO. The LVM is observed in samples that are grown with a

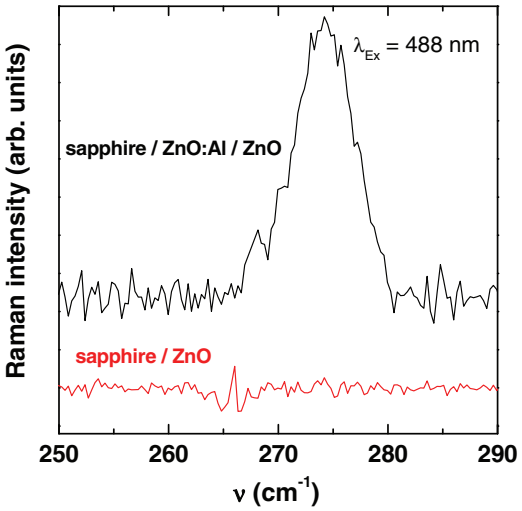

FIG. 2. (Color online) Raman backscattering spectra of ZnO deposited on c axis-oriented sapphire. The spectrum depicted in black was obtained from a specimen that contained a 200-nm-thick Al-doped layer between the undoped ZnO layer and the substrate. The Al concentration amounted to 2 at.%. Both samples were grown simultaneously.

c(+) face or Zn-termination. Moreover, this is consistent with the observation that homoepitaxial growth of nitrogen-doped ZnO on Zn-terminated single crystals gives rise to the LVM at $\nu \approx 274$ cm^{-1}, while on O-terminated single crystals, the LVM is undetectable.[15]

For the following experiments, all specimen were deposited on ZnO:Al-coated sapphire to promote the LVM at $\nu \approx 274$ cm^{-1}. The doped layer had a thickness of only $\approx$20 nm, whereas the thickness of the undoped ZnO layer amounted to ≈ 1 μm. Figure 3 shows Raman backscattering spectra measured at room temperature on isotopically enriched ZnO. When the natural Zn distribution is exchanged with

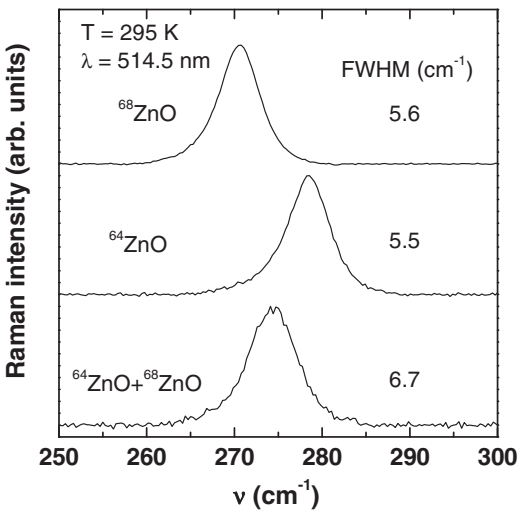

FIG. 3. Raman backscattering spectra of isotopically enriched ^{68}ZnO, ^{64}ZnO, and a one-to-one mixture of ^{68}ZnO and ^{64}ZnO. The data were measured at $T = 295$ K using an excitation wavelength of $\lambda = 514.5$ nm. FWHM indicates the full width at half maximum of the vibrational modes.

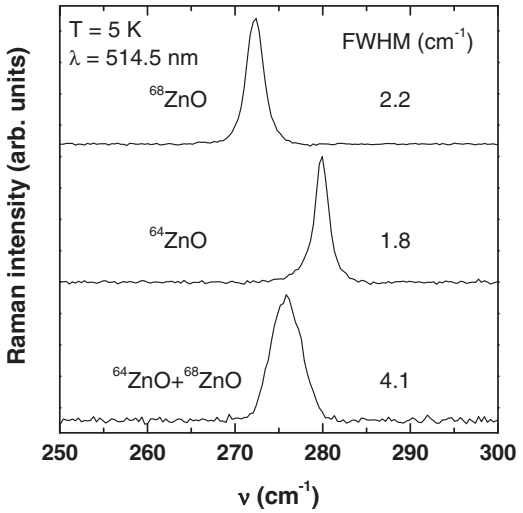

FIG. 4. Raman backscattering spectra of isotopically enriched ^{68}ZnO, ^{64}ZnO, and a one-to-one mixture of ^{68}ZnO and ^{64}ZnO. The data were measured at $T = 5$ K using an excitation wavelength of $\lambda = 514.5$ nm.

^{64}Zn and ^{68}Zn, the LVM is observed at $\nu = 278.6$ and 270.7 cm^{-1}, respectively, with a linewidth of 5.5 and 5.6 cm^{-1}. The difference in linewidth is caused by a small difference in the isotopic purity of the two samples. ^{64}ZnO and ^{68}ZnO had an isotopic enrichment of 99.2 and 98.0%, respectively. The sample that was grown from a 1:1 ratio of ^{64}ZnO and ^{68}ZnO reveals the LVM at $\nu = 274.4$ cm^{-1}. It is interesting to note that the linewidth of this specimen increases to 6.7 cm^{-1}.

In order to determine the intrinsic linewidth of the vibrational mode, the samples were cooled to $T = 5$ K, and it was ensured that the spectral resolution of the Raman setup was better than 1 cm^{-1}. The Raman spectra are plotted in Fig. 4. For ^{68}ZnO and ^{64}ZnO, the LVM is observed at 272.2 and 279.6 cm^{-1}, respectively, with a linewidth of 2.2 and 1.8 cm^{-1}. At 5 K, the difference in isotopic purity of the samples results in a line broadening of 0.4 cm^{-1}. On the other hand, the sample that was grown from a 1:1 ratio of ^{64}ZnO and ^{68}ZnO reveals a linewidth of 4.1 cm^{-1}, and the vibrational mode is located at $\nu = 275.8$ cm^{-1}.

The change of the vibrational frequency due to a change of the Zn isotope mass was determined for the data shown in Figs. 3 and 4. When ^{64}Zn is exchanged with ^{68}Zn, a shift of $\Delta\nu = 7.9$ and 7.5 cm^{-1} to smaller wave numbers is obtained at $T = 295$ and 5 K, respectively. When the LVM of ^{64}ZnO is compared to that of the sample composed of a 1:1 ratio of ^{64}ZnO and ^{68}ZnO, a shift of the LVM to smaller wave numbers is observed by $\Delta\nu = 4.2$ and 4.1 cm^{-1} at $T = 295$ and 5 K, respectively. The isotope frequency-shift can be calculated using the harmonic oscillator approach. The change of the frequency is given by

$$\Delta\nu = \nu(^{64}\mathrm{Zn})\left(1 - \sqrt{\frac{m(^{X}\mathrm{Zn})}{m(^{64}\mathrm{Zn})}}\right), \qquad (1)$$

where X specifies the Zn isotope and m represents its mass. The calculated frequency changes amount to $\Delta\nu = 8.3$ and 4.3 cm^{-1} for the samples with ^{68}Zn and a 1:1 ratio of ^{64}Zn and

TABLE I. Change of the vibrational frequency, $\Delta\nu$, for isotopically enriched ZnO samples. The experimental values were determined from Raman backscattering data shown in Fig. 4. The calculated values were obtained using the harmonic oscillator approach according to Eq. (1).

	$\lvert\Delta\nu\rvert$ (cm^{-1})		
Mass ratio, X	Experiment ($T = 295$ K)	Experiment ($T = 5$ K)	Model
^{64}ZnO/^{68}ZnO	7.9	7.5	8.3
^{64}ZnO/(^{64}ZnO + ^{68}ZnO)	4.2	4.1	4.3

^{68}Zn, respectively. These values are in excellent agreement with the experimental data (see Table I). This suggests that the origin of the LVM must be caused by a pure Zn vibration.

To investigate the influence of doping on the Zn-related vibrational mode, isotopically enriched specimens were doped with nitrogen. Doping was achieved by adding a flow of N_2O gas to the PLD process. The N concentration was determined from secondary ion mass spectrometry measurements and amounted to 1.3×10^{20} cm^{-3}. In Fig. 5, the Raman spectra of the N-doped ^{68}ZnO and ^{64}ZnO + ^{68}ZnO specimens are plotted with peak positions at 272.3 and 275.8 cm^{-1}, respectively, and a linewidth of 2.3 and 4.7 cm^{-1}. The data were taken at $T = 5$ K. It is important to note that the spectra are similar to those obtained from undoped samples (see Fig. 4). This clearly shows that doping does not influence the Zn-related LVM. Moreover, the data are not consistent with the idea that Zn_i-N_O complex are formed, because for the sample composed of ^{64}ZnO and ^{68}ZnO, one would expect two vibrational modes located at $\nu = 272.4$ and 279.9 cm^{-1}. However, only a single resonance is observed.

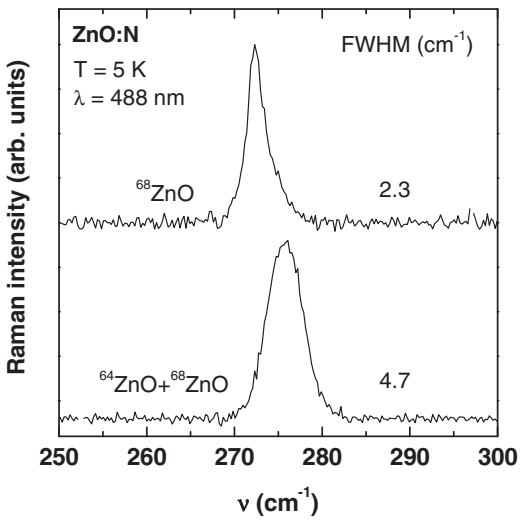

FIG. 5. Raman spectra of nitrogen-doped ZnO. The top spectrum was obtained on isotopically enriched ^{68}ZnO, and the bottom spectrum was measured on a sample that contained a one-to-one mixture of ^{68}ZnO and ^{64}ZnO. The nitrogen concentration amounted to [N] $\approx 1.4 \times 10^{20}$ cm^{-3}. The measurements were performed at 295 K, with an excitation wavelength of $\lambda = 488$ nm.

IV. DISCUSSION

The data presented in the previous section clearly shows that the appearance of the LVM at $\nu \approx 274$ cm^{-1} is directly related to the surface polarity of ZnO. Moreover, the appearance of the vibrational mode and its frequency are unrelated to the presence of dopants. The frequency shifts observed for isotopically enriched ZnO show that the LVM is caused by a pure Zn vibration. In this section, possible models are considered to account for the data. The models comprise a monomolecular model (Sec. IV A), a bimolecular model (Sec. IV B), and a zinc cluster model (Sec. IV C). Finally, in Sec. IV D, the stabilization of interstitial Zn clusters is discussed.

A. Monomolecular model

The data presented in Sec. III clearly show that the LVM at 275 cm^{-1} is caused by a pure Zn vibration. In the past, a microscopic model was proposed to account for the LVM. The model comprised an interstitial zinc atom bound to a substitutional nitrogen atom (Zn_i-N_O). Based on *ab initio* DFT calculations, two possible configurations for this complex were identified with a binding energy of about 0.9–0.94 eV. The calculated frequencies of the vibrational stretching modes of the Zn_i-N_O complex were in good agreement with the experimentally observed Zn-related LVM.[14] We extended this monomolecular model to other dopants in ZnO and to undoped ZnO. For this purpose, a supercell with 96 atoms was used, and the substitutional nitrogen atom of the interstitial Zn complex was replaced with P, Sb, or O. Then, the frequency of the vibrational stretching mode was calculated for each complex Zn_i-X_O; here X denotes the atom substituting a lattice oxygen. For antimony, the antisite configuration was also considered. The calculated frequencies along with experimentally determined values for the LVMs are summarized in Table II. The experimental data show that the introduction of dopants does not lead to a significant shift of the vibrational mode. On the other hand, the calculated frequency of the interstitial Zn complex is very sensitive to type of dopants. The calculated vibrational frequencies vary between $\nu = 220$ and 276 cm^{-1}. A good agreement between the measured and calculated frequency is obtained only for the Zn_i-N_O complex, which is consistent with a previous publication.[14]

The nitrogen-doped ZnO sample that was grown from a target with a 1:1 ratio of ^{64}ZnO and ^{68}ZnO showed only

TABLE II. Frequency of the Zn-related LVM in doped and undoped ZnO. Details on the DFT calculations are described in the text.

	Vibrational frequency (cm^{-1})	
Dopant	Experiment	Theory
N	274.1	276
P	–	237
Sb on Zn site	277 (Ref 10)	269
Sb on O site	–	221
Undoped	274.1	224

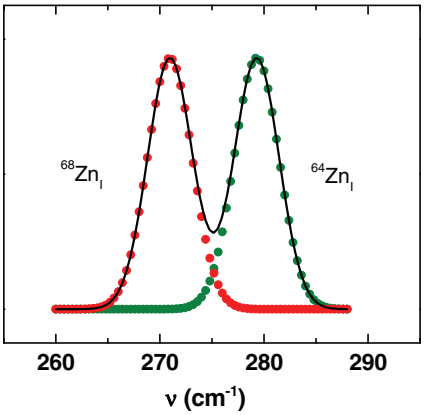

FIG. 6. (Color online) Monomolecular model: depiction of the expected LVMs for a ZnO sample composed of equal amounts of ^{64}ZnO and ^{68}ZnO. Position and linewidth were taken from the experimental data.

one broad LVM at $\nu = 275.8$ cm^{-1} (see Fig. 5). However, when employing the monomolecular model, where the origin of the LVM is assumed to be the stretching vibration of Zn_i-N_O complexes, a completely different line shape should be obtained. The presence of two Zn isotopes should give rise to two well-separated LVMs as depicted in Fig. 6. The data were obtained by plotting two Gaussian lines using the experimentally determined linewidth and vibrational frequency at room temperature. A comparison of Fig. 6 with the Raman spectra of N-doped ZnO (see Fig. 5) clearly shows that the LVM cannot be due to the stretching vibration of Zn_i-N_O complexes. Hence, the recently proposed monomolecular model[14] has to be ruled out.

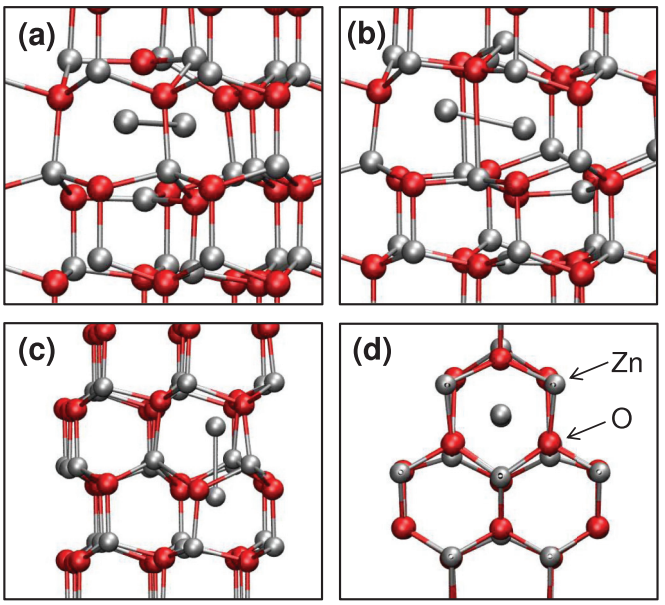

FIG. 7. (Color online) Calculated atomic position of interstitial zinc molecules, Zn_i-Zn_i, in a ZnO supercell consisting of 96 atoms. (a) and (b) show two stable configurations for Zn_i-Zn_i parallel to the basal plain. The calculated vibrational frequencies amounted to $\nu = 270$ and 272 cm^{-1}. (c) and (d) depict the position of the molecule parallel to the c axis with a vibrational frequency of $\nu = 264$ cm^{-1}.

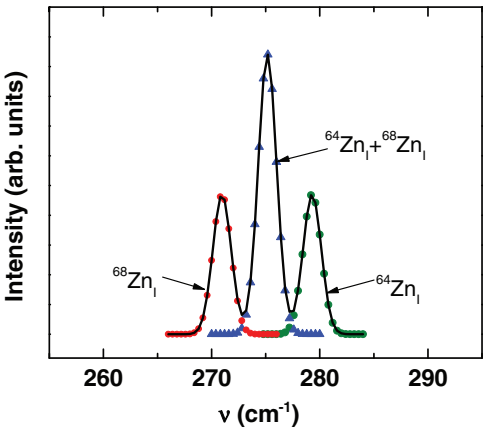

FIG. 8. (Color online) Bimolecular model: depiction of the expected LVMs in a ZnO sample composed of equal amounts of ^{64}ZnO and ^{68}ZnO. In this case, $^{64}Zn_2$, $^{64}Zn^{68}Zn$, and $^{68}Zn_2$ molecules form with a 1 : 2 : 1 concentration ratio. The position of the lines and their linewidth were taken from the experimental data.

B. Bimolecular model

An attractive alternative to the monomolecular model is based on the idea that interstitial Zn atoms could combine to molecules. The expected isotopic shift of the stretching frequency is consistent with the experimental data, since the vibration is caused by zinc atoms only. Zn molecules can be accommodated parallel to the basal plane or along the c axis in the interstitial lattice. For the former configuration, two stable positions were identified using DFT calculations [see Figs. 7(a) and 7(b)]. Both configurations have in common that the interstitial Zn molecule causes the breaking of a Zn-O bond and a pronounced displacement of the Zn and O atoms towards the interstitial lattice. The breaking of Zn-O bonds is consistent with the observation of the phonon mode at $\nu = 577.0$ cm^{-1}, which was ascribed to a resonant enhancement of the E_1 and A_1 LO phonons in ZnO due to extrinsic Fröhlich scattering.[12] In addition, some displacement

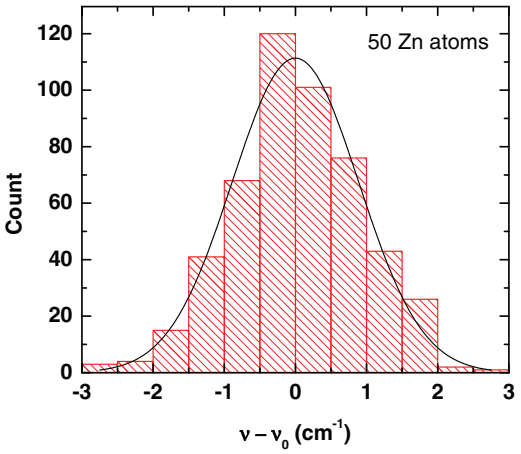

FIG. 9. (Color online) Histogram of the calculated vibrational frequencies, ν-ν_0, for a linear chain of 50 zinc atoms with an equal amount of ^{64}Zn and ^{68}Zn. 500 calculations were performed with random permutations of the Zn isotopes. The solid line represents a Gaussian fit to the data with a linewidth of $\Delta\nu \approx 2.1$ cm^{-1}.

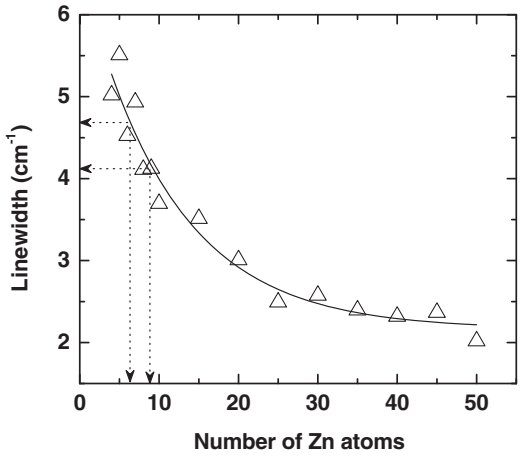

FIG. 10. Linewidth of the frequency distributions as a function of the length of the liner chain. The zinc clusters contained equal concentrations of ^{64}Zn and ^{68}Zn that were randomly distributed. The arrows indicate the experimentally observed linewidth of 4.1–4.7 cm^{-1} and the corresponding cluster size.

of nearest-neighbor atoms is also observed. The frequencies of the stretching vibrations were determined from force-constant calculations. For the configurations shown in Figs. 7(a) and 7(b), vibrational frequencies of $\nu = 270$ and 272 cm^{-1} were obtained, respectively. When the interstitial Zn molecule is accommodated parallel to the c axis only, minor displacement of the nearest-neighbor atoms is observed [Figs. 7(c) and 7(d)]. A calculation of the stretching frequency yielded $\nu = 264$ cm^{-1}. The calculated vibrational frequencies are in good agreement with the experimental data, indicating that the microscopic origin of the vibrational mode at $\nu = 274$ cm^{-1} might be caused by the presence of interstitial Zn molecules.

The validity of the bimolecular model can be tested in a Zn isotope experiment. When ZnO samples are grown from a target that is composed of a 1:1 ratio of ^{64}ZnO and ^{68}ZnO, interstitial molecules with three different masses are expected to form, namely, ^{64}Zn$_2$, ^{64}Zn^{68}Zn, and ^{68}Zn$_2$ with a concentration ratio of 1 : 2 : 1. Hence, in the experiment three well-separated vibrational modes should be observed with an intensity ratio of 1 : 2 : 1. To estimate the expected line shape, Gaussian lines were plotted using the experimentally determined linewidth of about 2 cm^{-1}, and the frequencies of the mode observed in ^{64}ZnO and ^{68}ZnO (see Fig. 4). To determine the position of the mode composed of ^{64}Zn^{68}Zn, the isotopic shift was calculated using the harmonic oscillator approach. The expected line shape based on the bimolecular model is shown in Fig. 8. However, the experimental data shown in Fig. 4 differs significantly. For the sample composed of a 1:1 ratio of ^{64}ZnO and ^{68}ZnO, only a single vibrational mode is observed. Interestingly, however, the linewidth is twice as large ($\Delta\nu \approx 4.1$ cm^{-1}) compared to the ZnO samples that contain only one Zn isotope. Hence, this clearly shows that the bimolecular model cannot account for the experimental data.

C. Zinc clusters

Despite the fact that the mono- and bimolecular models cannot account for the experimental data, the isotope experiments shown in Sec. III clearly establish that the LVM at 274 cm^{-1} is caused by a pure zinc vibration. Moreover, the presence of two zinc isotopes in the specimens gives rise to line broadening. This suggests that the underlying mechanism might be caused by Zn clusters that form during growth on the c(+) face or Zn-terminated surface. To explore this direction, the eigenmodes of small Zn clusters containing 5 to 50 atoms were calculated. Since the exact structure of the Zn clusters is unknown DFT cannot be used to determine their vibrational properties. However, the influence of isotopes on the linewidth of a vibrational mode can be estimated using a simple linear chain model. Zn atoms were placed in a linear chain with a random distribution of ^{64}Zn and ^{68}Zn, while maintaining an equal concentration of both isotopes. Then the eigenmodes of the clusters were calculated allowing only nearest-neighbor interaction. For each cluster size, 500 calculations were performed with random permutations of the Zn isotopes. As an example, the frequency distribution in a chain containing 50 atoms is plotted in Fig. 9. A fit of the data to a Gaussian distribution yielded a linewidth of $\Delta\nu \approx 2.1$ cm^{-1}. The frequency distributions for all Zn cluster sizes were analyzed in the same way, and then the obtained linewidths were plotted as a function of the number of Zn atoms in the linear chain (Fig. 10). When the cluster is composed

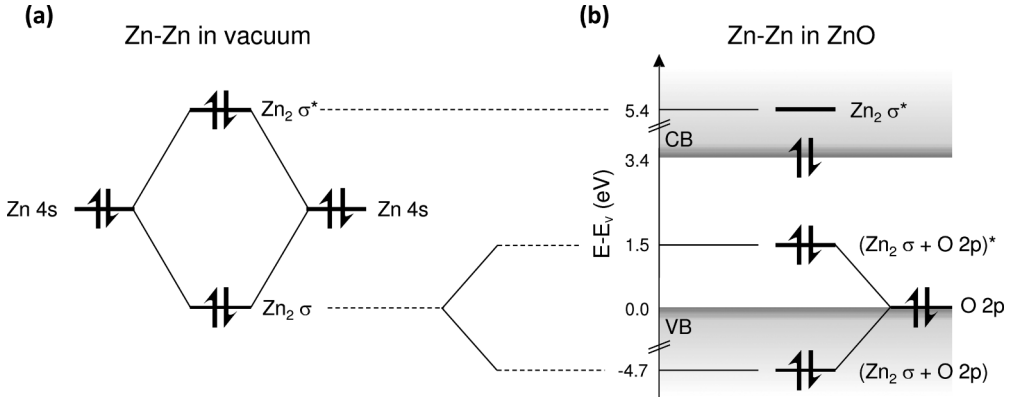

FIG. 11. Schematic depiction of the energy levels of a Zn-Zn molecule in vacuum (a). Bonding (σ) and antibonding orbitals (σ^*) are fully occupied. (b) Shows the energy levels of a Zn-Zn molecule in the ZnO lattice [see Fig. 7(a)]. For the calculation of the energy levels, HSE hybrid functionals were used.[18] VB and CB denote the valence and conduction band, respectively. Details are described in the text.

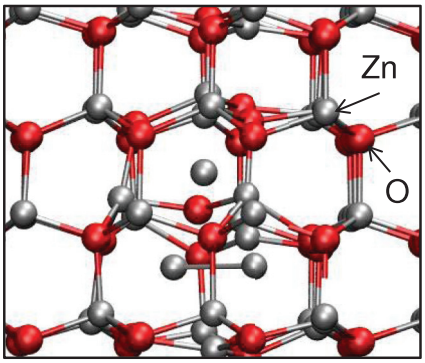

FIG. 12. (Color online) Calculated atomic position of an interstitial zinc cluster consisting of $n = 3$ atoms. A ZnO supercell consisting of 128 atoms was used for the calculations.

of only a few atoms, the linewidth is large and exceeds 5 cm^{-1}. However, with an increasing number of Zn atoms in the cluster, the linewidth decreases and asymptotically approaches a residual value of about 2.2 cm^{-1}.

Raman scattering performed on the sample that was grown from a 1:1 ratio of ^{64}ZnO and ^{68}ZnO yielded a linewidth of 4.1–4.7 cm^{-1} for the vibrational mode (see Figs. 4 and 5). According to the data shown in Fig. 10, such a linewidth is expected for clusters composed of about six to nine Zn atoms. Hence, our data suggest that the LVM at $\nu = 274$ cm^{-1} originates from small zinc inclusions that form under Zn-rich growth conditions. It is conceivable that the Zn inclusions form in vacancies and/or small vacancy clusters that limit their size.

D. Stabilization of zinc clusters

In contrast to covalent bonding, the nature of metallic bonding is collective. In most metals, bonding occurs because the delocalized conduction electrons are electrostatically attracted to the positively charged metal ions. Therefore, a zinc molecule or small cluster consisting of only a few Zn atoms would not be stable. In the following, we consider small Zn clusters with an even and an odd number of Zn atoms; e.g., $n = 2$ and 3. The molecular orbitals of a Zn molecule ($n = 2$) and their occupation are depicted in Fig. 11 Since the bonding (σ) and antibonding orbitals (σ^*) are fully occupied, the Zn molecule is destabilized.

The bonding configurations and energetic positions of the molecular orbitals of interstitial Zn molecules and small clusters were investigated using DFT calculations. Since standard DFT calculations suffer from the well-known band-gap error, we employed hybrid functionals of HSE,[18] as described in Sec. II. When a Zn molecule is accommodated parallel to the basal plane of ZnO (see Fig. 7), the Zn_2 σ orbital hybridizes with O $2p$ orbitals and forms a bonding (Zn_2 $\sigma + O$ $2p$) and an antibonding (Zn_2 $\sigma + O$ $2p$)* orbital [see Fig. 11(b)]. The bonding orbital is located in the valence band at $E - E_V = -4.7$ eV, while the antibonding orbital resides in the band gap at $E - E_V = 1.5$ eV. These orbitals are fully occupied. On the other hand, the antibonding Zn_2 σ^* orbital is located deep in the conduction band at $E - E_V = 5.4$ eV. Consequently, the charge that would occupy the antibonding σ^* orbital is transferred to the conduction-band minimum, thereby stabilizing the interstitial Zn molecule and rendering it a shallow donor complex.

The microscopic configuration for a Zn cluster with three interstitial Zn atoms is depicted in Fig. 12. Two of the Zn atoms form a molecule, while the third Zn atom resides about 2.4 Å above the molecule. Note that the accommodation of three interstitial Zn atoms results in a pronounced lattice distortion and a breaking of a Zn-O bond. For this configuration, the energetic positions of the molecular orbitals were calculated using hybrid functionals. The bonding orbitals of all interstitial Zn atoms hybridize with oxygen $2p$ orbitals. The resulting bonding orbitals are located at $E - E_V = -5.3$ eV. The corresponding antibonding orbitals reside in the band gap of ZnO and are located at $E - E_V = 1.0$ eV and $E - E_V = 2.4$ eV (see Fig. 13). Similar to the interstitial Zn molecule, the (Zn_i-Zn_i) antibonding orbital σ^* is located deep in the conduction band at $E - E_V = 4.7$ eV, and the charge is transferred to the conduction-band minimum. Hence, an odd number of interstitial Zn atoms also causes n-type doping and introduces localized states in the band gap of ZnO. The calculation shows that small Zn clusters are stable in ZnO,

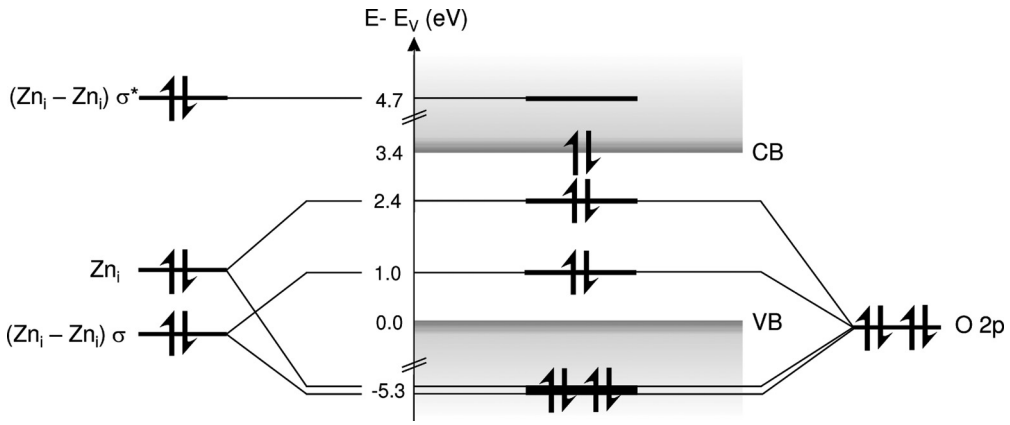

FIG. 13. Schematic depiction of the molecular orbitals of an interstitial Zn cluster consisting of $n = 3$ atoms (see Fig. 12). The bonding orbital (σ) of the interstitial molecule hybridizes with oxygen $2p$ orbitals and with the third interstitial Zn atom. For the calculation of the energy levels, HSE hybrid functionals were used (Ref. 18). VB and CB denote the valence and conduction band, respectively. Details are described in the text.

cause n-type conductivity, and therefore are consistent with our experimental observations.

V. SUMMARY

In summary, we have performed Raman backscattering measurements on ZnO thin films that were deposited from natural ZnO and isotopically enriched ^{64}ZnO and ^{68}ZnO targets. The presence of the LVM at $\nu \approx 274$ cm^{-1} is directly related to the surface polarity of ZnO. The LVM is observed only in samples that are grown with a c(+) face or Zn termination. Adding oxygen from a plasma source during growth suppresses the LVM, indicating that the growth conditions without the presence of additional oxygen are Zn rich. In isotopically pure ^{64}ZnO and ^{68}ZnO, the controversially discussed LVM is observed at 279.6 and 272.2 cm^{-1}, respectively, with a linewidth of 2.2 and 1.8 cm^{-1}. When the specimen contained equal amounts of ^{64}Zn and ^{68}Zn, the vibrational mode is located at $\nu = 275.8$ cm^{-1}, and the linewidth amounts to 4.1 cm^{-1}. The isotopic shift for ^{64}ZnO and ^{68}ZnO amounted to 7.5 cm^{-1}, and a value of 4.2 cm^{-1} was measured for the isotopic shift of ^{64}ZnO to ^{64}ZnO + ^{68}ZnO. Using the harmonic oscillator approach, the isotopic frequency ratios were calculated. The resulting isotopic shifts amounted to 8.3 and 4.3 cm^{-1} for ^{64}ZnO to ^{68}ZnO and for ^{64}ZnO to ^{64}ZnO + ^{68}ZnO, respectively. They are in excellent agreement with the experimental data and show that the origin of the vibrational mode at $\nu \approx 274$ cm^{-1} is due to Zn vibrations. The data were discussed in terms of a monomolecular, bimolecular, and cluster model. However, only the Zn cluster model is consistent with the data. To account for the linewidth observed in samples grown from a 1:1 ratio of ^{64}ZnO and ^{68}ZnO, this model predicts that the vibrational mode occurs from small Zn clusters composed of about 6 to 9 Zn atoms. According to DFT calculations, small Zn clusters are stable in ZnO since the antibonding orbitals are in resonance with the conduction band and, hence, transfer their charge to the conduction band edge.

ACKNOWLEDGMENTS

The authors acknowledge financial support from the Bundesministerium für Umwelt, Naturschutz und Reaktorsicherheit under Grant No. 0325446A.

[1] N. H. Nickel and E. Terukov, *Zinc Oxide—A Material for Micro- and Optoelectronic Applications* (Springer, New York, 2005).
[2] J. Wager, Science **300**, 1245 (2003).
[3] A. Tsukazaki, A. Ohtomo, T. Onuma, M. Ohtani, T. Makino, M. Sumiya, K. Ohtani, S. F. Chichibu, S. Fuke, Y. Segawa, H. Ohno, H. Koinuma, and M. Kawasaki, Nat. Mater. **4**, 42 (2005).
[4] S. Major and K. L. Chopra, Sol. Energy Mater. **17**, 319 (1988).
[5] A. Janotti and C. G. Van de Walle, Nat. Mater. **6**, 44 (2007).
[6] C. G. Van de Walle, Phys. Rev. Lett. **85**, 1012 (2000).
[7] D. M. Hofmann, A. Hofstaetter, F. Leiter, H. Zhou, F. Henecker, B. K. Meyer, S. B. Orlinskii, J. Schmidt, and P. G. Baranov, Phys. Rev. Lett. **88**, 045504 (2002).
[8] D. C. Look, J. W. Hemsky, and J. R. Sizelove, Phys. Rev. Lett. **82**, 2552 (1999).
[9] A. Kaschner, U. Haboeck, M. Strassburg, G. Kaczmarczyk, A. Hoffmann, C. Thomsen, A. Zeuner, H. R. Alves, D. M. Hofmann, and B. K. Meyer, Appl. Phys. Lett. **80**, 1909 (2002).
[10] C. Bundesmann, N. Ashkenov, M. Schubert, D. Spemann, T. Butz, E. M. Kaidashev, M. Lorenz, and M. Grundmann, Appl. Phys. Lett. **83**, 1974 (2003).
[11] F. J. Manjón, B. Marí, J. Serrano, and A. H. Romero, J. Appl. Phys. **97**, 053516 (2005).
[12] F. Friedrich and N. H. Nickel, Appl. Phys. Lett. **91**, 111903 (2007).
[13] L. Artús, R. Cuscó, E. Alarcón-Lladó, G. González-Díaz, I. Mártil, J. Jiménez, B. Wang, and M. Callahan, Appl. Phys. Lett. **90**, 181911 (2007).
[14] F. Friedrich, M. A. Gluba, and N. H. Nickel, Appl. Phys. Lett. **95**, 141903 (2009).
[15] N. Hanèche, A. Lusson, C. Sartel, A. Marzouki, V. Sallet, M. Oueslati, F. Jomard, and P. Galtier, Phys. Status Solidi B **247**, 1671 (2010).
[16] V. I. Anisimov, F. Aryasetiawan, and A. Lichtenstein, J. Phys.: Condens. Matter **9**, 767 (1997).
[17] A. Janotti, D. Segev, and C. G. Van de Walle, Phys. Rev. B **74**, 045202 (2006).
[18] J. Heyd, G. E. Scuseria, and M. Ernzerhof, J. Chem. Phys. **118**, 8207 (2003).
[19] J. P. Perdew, K. Burke, and M. Ernzerhof, Phys. Rev. Lett. **77**, 3865 (1996).
[20] G. Kresse and J. Furthmüller, Phys. Rev. B **54**, 11169 (1996).
[21] G. Kresse and D. Joubert, Phys. Rev. B **59**, 1758 (1999).
[22] A. Janotti and Chris G. Van de Walle, Phys. Rev. B **76**, 165202 (2007).
[23] Y. Adachi, N. Ohashi, T. Ohnishi, T. Ohgaki, I. Sakaguchi, H. Haneda, and M. Lippmaa, J. Mater. Res. **23**, 3269 (2008).